Self-consistent field theory of the strongly stretched dry polymer brush

Willem Gispen

Supervised by Andreas Münch

University of Oxford

A thesis submitted for the degree of

MSc in Mathematical and Theoretical Physics

Trinity 2019

Abstract

There is some numerical evidence that the self-consistent field theory (SCFT) for dry polymer brushes converges to the strong stretching theory (SST) in the limit of strong stretching [8]. However, the numerical results are restricted to moderately stretched brushes. We insert the SST prediction for the self-consistent field into the diffusion equations of SCFT and analyse them in the strong stretching limit using asymptotic analysis. The resulting asymptotic solution for the segment density ϕ shows that the self-consistency relation $\phi = 1$ is not satisfied, not even approximately. Therefore, any future asymptotic treatment should include corrections to the SST prediction. Nevertheless, our asymptotic analysis is the first step towards asymptotic evidence that the SCFT converges to SST in the strong stretching limit.

Contents

Introduction **4**
Outline 5

1 Self-consistent field theory of the dry polymer brush **6**
1.1 Definition of the dry polymer brush 6
1.1.1 Continuous Gaussian chain in an external field 6
1.1.2 The dry polymer brush 7
1.2 The self-consistent field approximation 9
1.2.1 The self-consistent field approximation 9
1.2.2 Exploiting the planar symmetry of the brush 11
1.3 The strongly stretched dry brush 11
1.3.1 Strong stretching theory 13
1.4 The diffusion equations 14
1.4.1 Boundary conditions 15

2 Investigation of the diffusion equations with parabolic potential in the strong stretching limit **17**
2.1 Asymptotic solution 17
2.1.1 Transforming the diffusion equations 18
2.1.2 Asymptotic solution for u 19
2.1.3 Asymptotic solution for u^* 22
2.1.4 Asymptotic solution for ϕ 23
2.2 Numerical solution 26
2.3 Comparison of asymptotic and numerical solutions 27
2.3.1 Comparison of the segment density 28
2.3.2 Comparison of the outer solutions for u and u^* 28
2.3.3 Comparison of composite solutions 31

3 Discussion and outlook **33**
3.1 Re-examining the parabolic potential 33
3.2 Outlook 35

References **36**

Introduction

Polymers form an ubiquitous class of materials. Examples are synthetic materials such as plastics and rubbers, and natural materials such as wool, proteins and DNA. Polymers are also present in personal care products, paints and processed foods. Polymers are popular as an industrial material because they can be cheap, easy to process, and display a large flexibility in their material properties.

This flexibility is due to their large variety of design parameters. Material design is usually done by producing a large amount of different samples with slightly different design parameters. The desired material properties are then tested experimentally. Because the design parameter space is enormous, this method is expensive and inefficient. Therefore accurate theoretical methods may be helpful to understand which parameters are important and how they should be chosen. In short, polymer modelling can be helpful when designing a new polymeric material [9].

The self-consistent field theory (SCFT) initiated by Edwards [1] in 1965 "has a track record to rival any and all theories in soft condensed matter physics" [10]. Although SCFT can be applied to virtually any equilibrium polymer system [10], it is particularly accurate when each polymer chain is in contact with a large number of other chains. This is the case with, for example, highly concentrated polymer solutions and high-molecular-weight polymer melts. In other situations, such as dilute polymer solutions, different techniques such as the renormalisation group or field-theoretic simulations need to be considered [9]. Another possible downside of SCFT is that it requires numerical methods.

The strong stretching theory (SST) introduced by Semenov [3] in 1985 is an approximation of the SCFT applicable to stretched polymers. The SST gives simple closed-form formulas for quantities of interest, which makes it easier to understand systems intuitively and qualitatively. However, SST is often inaccurate for realistic

experimental conditions [10]. Numerous papers have been written about the main corrections to SST, partly to provide improved closed-form approximations, and partly to understand the accuracy of SST. Nonetheless, there is no well-defined approach to these "finite stretching corrections" [8].

Perturbation theory with the stretching as the large parameter could provide a systematic approach to finite stretching corrections. Ideally, this approach would lead to more rigorous constraints/bounds on the finite stretching corrections, as opposed to the current corrections based on physical intuition or numerical experimentation and validation. These constraints could at the same time give conclusive evidence on the accuracy of the SST in the strong-stretching limit.

We have chosen the so-called "dry polymer brush" as the testing ground of this perturbative approach, because the dry polymer brush is a simple but non-trivial polymer system, whose SST and most important finite stretching corrections are known numerically [8]. Apart from this, brushes are important themselves: they can modify surface properties such as friction, wetting and adhesion, and help our understanding of block copolymers [10].

Outline

We start this thesis by explaining both the SCFT and the SST of the dry polymer brush in Chapter 1. Our presentation is adapted from a handbook by Matsen [10].

Then in Chapter 2 we test, with numerical and asymptotic analysis, to what extent the SST prediction for the self-consistent field is indeed self-consistent in the strong stretching limit. To the best of our knowledge, the asymptotic analysis has not been done before.

Finally in Chapter 3 we discuss what we have learned and how to continue.

Chapter 1
Self-consistent field theory of the dry polymer brush

In this chapter we will present the self-consistent field theory (SCFT) formalism for the so-called "dry polymer brush". We start by defining the dry polymer brush, and then develop the SCFT in Section 1.2. Next, we present the strong stretching approximation in Section 1.3, and finish with the diffusion equations for SCFT in Section 1.4. Our presentation is adapted from a handbook by Matsen[10].

1.1 Definition of the dry polymer brush

We model the brush as a collection of individual polymer chains, so we first need to model a single chain. To do this, we use the continuous Gaussian chain model.

1.1.1 Continuous Gaussian chain in an external field

A polymer chain is modelled using the continuous Gaussian chain model, which firstly means that its position is parametrised by a differentiable function $\boldsymbol{r}(s)$ of a continuous parameter $s \in [0, 1]$. The physical interpretation of the parametrisation parameter s is that s-intervals of equal length have equal mass. [1]

Secondly, the continuous Gaussian chain model incorporates an entropic stretching energy [2] proportional to $|\boldsymbol{r}\,'(s)|^2$. Lastly we can include an external field $W(\boldsymbol{r})$.

[1] Conventionally, s is chosen in $[0, N]$. In this case, N is the number of "course-grained segments", each of which have a segment length b (see for example [9]). We use $s \in [0, 1]$ and the radius of gyration R_g instead, which in the segment language becomes $R_g = \sqrt{6}Nb^{1/2}$.

[2] The segment language of footnote 1 is useful to explain why this stretching energy is entropic and why it is proportional to $|\boldsymbol{r}\,'(s)|^2$. Here we take the continuous Gaussian chain model for granted.

Combining these two energies, a piece $[s_1, s_2]$ of the chain $\boldsymbol{r}(s)$ has energy

$$E[\boldsymbol{r}, s_1, s_2] = \int_{s_1}^{s_2} ds \left(\frac{|\boldsymbol{r}\,'(s)|^2}{4R_g^2} + W(\boldsymbol{r}(s)) \right). \tag{1.1}$$

This energy is non-dimensional, i.e. we have set $k_B T = 1$ which we will do throughout this thesis. Furthermore R_g^2 is the squared radius of gyration. The radius of gyration R_g is a characteristic size of the free Gaussian polymer chain. More precisely, it is the average root-mean-squared distance of the polymer from its centre of mass. Therefore, R_g^3 is the characteristic volume spanned by the free chain. This must be contrasted with the volume v that the chain actually occupies.

All equilibrium properties of the Gaussian chain are then determined by the canonical partition function $Q[w]$ defined by

$$Q[W] \propto \int \widetilde{\mathcal{D}}\boldsymbol{r} \, \exp\left(- \int_0^1 ds \, W(\boldsymbol{r}(s)) \right), \tag{1.2a}$$

$$\widetilde{\mathcal{D}}\boldsymbol{r} \equiv \exp\left(- \int_0^1 ds \, \frac{|\boldsymbol{r}\,'(s)|^2}{4R_g^2} \right) \mathcal{D}\boldsymbol{r}. \tag{1.2b}$$

Here the factor (1.2b) incorporates the Boltzmann factor due to the stretching energy and $\mathcal{D}\boldsymbol{r}$ is the measure of functional integration over all paths $\boldsymbol{r}(s)$.[3]

1.1.2 The dry polymer brush

To model the brush, we use n identical continuous Gaussian chains $\boldsymbol{r}_\alpha(s) = (x_\alpha, y_\alpha, z_\alpha)(s)$ labelled by $\alpha = 1, \ldots, n$. The chains are identical in the sense that they each have the same radius of gyration R_g and the same occupied volume v. Then the molecules are grafted to the surface $x = 0$ of area A, which means we must enforce $x_\alpha(1) = 0$ for each molecule α. We also assume that the grafting density n/A of chains is so

[3]Normally we need to include kinetic energy and an integral over momentum. In this case, however, this only results in an irrelevant constant proportionality factor in the partition function[2].

high, that the brush is translationally invariant in the y and z directions.

The main further assumption of the dry polymer brush is that the chains together do not overlap nor leave any open space. To be precise, we assume that the brush has uniform "microscopic segment density" $\hat{\phi} = 1$, where

$$\hat{\phi}(\boldsymbol{r}) \equiv v \sum_{\alpha=1}^{n} \int_0^1 ds\, \delta(\boldsymbol{r} - \boldsymbol{r}_\alpha(s)). \tag{1.3}$$

The microscopic segment density $\hat{\phi}$ can be interpreted as the local fraction of space occupied by the polymer, so $\hat{\phi} = 1$ requires the polymer to fill all available space. Integrating $\hat{\phi} = 1$ over the volume AL of the brush gives that the brush length L is determined by the total volume nv of the chains as $AL = nv$.

Effectively, the only interaction between the chains is in the requirement of uniform microscopic segment density. Therefore, the canonical partition function of the brush Z is almost entirely decoupled. It is (see previous footnote 3)

$$Z \propto \int \left(\prod_\alpha \widetilde{\mathcal{D}}\boldsymbol{r}_\alpha\, \delta(x_\alpha(1)) \right) \delta[1 - \hat{\phi}]. \tag{1.4}$$

Here the factor $\delta[1-\hat{\phi}]$ is a functional delta function that ensures that the microscopic segment density is uniform i.e. that $\hat{\phi}(\boldsymbol{r}) = 1$ for every $\boldsymbol{r}$, and $\delta(x_\alpha(1))$ is a normal delta function that ensures that the end of each chain is grafted to the substrate at $x = 0$. Since all equilibrium properties of the brush are determined by Z, our task is to calculate Z. At the same time the definition (1.4) of Z completes the definition of the dry polymer brush.

1.2 The self-consistent field approximation

Unfortunately, we cannot calculate the partition function Z (1.4) exactly. To obtain analytic results, we must resort to approximations. The first of these is the self-consistent field approximation discussed in this section, the second is the strong stretching approximation discussed in Section 1.3.

1.2.1 The self-consistent field approximation

To start with, we use the integral representation of the δ-functional

$$\delta[1-\hat{\phi}] \propto \int \mathcal{D}W \exp\left(-v\int d\boldsymbol{r}\, W(\boldsymbol{r})(1-\hat{\phi})\right). \tag{1.5}$$

where the fields $W(\boldsymbol{r})$ are purely imaginary. This is just the functional analogue of the identity $\delta(x) = \frac{1}{2\pi}\int dk\, e^{ikx}$. Inserting (1.3) and (1.5) into (1.4) decouples the $\mathcal{D}\boldsymbol{r}_\alpha$ integrals, giving

$$Z \propto \int \mathcal{D}W \exp\left(-F[W]\right) \tag{1.6}$$

where for clarity we have defined

$$\frac{F[W]}{n} \equiv -\ln\left(\frac{Q[W]}{A}\right) - \frac{1}{AL}\int d\boldsymbol{r}\, W(\boldsymbol{r}), \tag{1.7a}$$

$$Q[W] \propto \int \widetilde{\mathcal{D}}\boldsymbol{r} \exp\left(-\int_0^1 ds\, W(\boldsymbol{r}(s))\right)\delta(x(1)). \tag{1.7b}$$

The factor $Q[W]$ is the partition function (1.2a) of a single polymer chain in a field W apart from the factor $\delta(x(1))$ which ensures the grafting of the chain.

Now comes the key "self-consistent field approximation": we approximate the integral (1.6) over $\mathcal{D}W$ with the dominant contribution from the self-consistent field

w. We do this using the saddle point method, so the SCFT approximation of (1.6) is

$$Z \approx \exp(-F[w])$$

where the self-consistent field w is defined as the saddle point of $F[W]$, i.e. the point where $\mathcal{D}F[W]/\mathcal{D}W = 0$. Inserting the definition (1.7a) of $F[W]$ into this saddle point equation gives the definition of the self-consistent field w: it is the field w such that

$$-AL \left.\frac{\mathcal{D}\ln(Q[W])}{\mathcal{D}W}\right|_{w(\boldsymbol{r})} = 1. \tag{1.8}$$

To make this condition more insightful, we define $\phi(\boldsymbol{r})$ as the average of the microscopic segment concentration $\hat{\phi}$ of n polymers in a field $W(\boldsymbol{r})$ i.e.

$$\phi[W](\boldsymbol{r}) \equiv \frac{1}{Q[W]} \int \widetilde{\mathcal{D}}\boldsymbol{r}\, \hat{\phi}(\boldsymbol{r}) \exp\left(-\int_0^1 ds\, W(\boldsymbol{r}(s))\right) \delta(x(1)) \tag{1.9}$$

where $\hat{\phi}$ is given by (1.3). We will refer to ϕ as "the segment density" from now on, as opposed to the microscopic segment density $\hat{\phi}$. The segment density ϕ can be expressed as

$$\phi[W](\boldsymbol{r}) = -AL \left.\frac{\mathcal{D}\ln(Q[W])}{\mathcal{D}W}\right|_{W(\boldsymbol{r})}.$$

So the condition (1.8) translates into the following: the self-consistent field is defined as the field $w(\boldsymbol{r})$ such that

$$\phi[w] = 1, \tag{1.10}$$

where the segment density ϕ is defined by (1.9).

So to calculate the partition function Z with self-consistent field theory we should take two steps: firstly, find the self-consistent field w that makes sure that $\phi = 1$, and secondly, calculate the free energy $F[w]$ from (1.7a).

1.2.2 Exploiting the planar symmetry of the brush

The self-consistent field approximation conveniently approximated n coupled path integrals with one path integral (1.7b). A further simplification arises from the symmetry of the brush: we have assumed that the brush is translationally invariant in the y and z directions. This means that both the self-consistent field $w(\boldsymbol{r})$ and the segment density $\phi(\boldsymbol{r})$ can only depend on the x-coordinate.

Therefore, the different components x, y and z of the chains in (1.7b) decouple. Since the y and z components are unaffected by the field $W(x)$, they only give trivial multiplicative factors, giving

$$Q[W] \propto A \int \widetilde{\mathcal{D}}x(s) \exp\left(-\int_0^1 ds\, W(x(s))\right) \delta(x(1)). \tag{1.11a}$$

$$\phi[W](\boldsymbol{r}) \equiv \frac{1}{Q[W]} \int \widetilde{\mathcal{D}}x\, \hat{\phi}(x) \exp\left(-\int_0^1 ds\, W(x(s))\right) \delta(x(1)) \tag{1.11b}$$

Thus we are looking for the self-consistent field $w(x)$ such that the segment density $\phi(x)$ determined by (1.11) satisfies $\phi = 1$. The only thing we need is a convenient manner of calculating the path integrals (1.11). In Section 1.3 the partition function $Q[W]$ is approximated using the strong stretching theory (SST), while in Section 1.4 a computational method is presented that uses diffusion equations.

1.3 The strongly stretched dry brush

We now turn to the specific case of the strongly stretched dry brush. In this case, we can make a simplification known as the strong stretching theory (SST), allowing us to approximate the self-consistent field w and the free energy F of the brush.

Before presenting the SST, we introduce the perturbation parameter ϵ:

$$\epsilon = R_g/L.$$

So ϵ measures the extent to which the polymer chains are stretched, more precisely the ratio between their natural length scale R_g and their actual extension L in the brush. Now the strongly stretched dry brush is defined as a dry brush for which $\epsilon \ll 1$. To take advantage of the perturbation parameter, we non-dimensionalise x and rescale W as

$$x = L\tilde{x}, \quad W = \frac{\mu}{\epsilon^2}.$$

In this language the energy becomes (dropping the tilde)

$$E[x(s), s_1, s_2] = \frac{1}{\epsilon^2} \int_{s_1}^{s_2} ds \left(\frac{|x'(s)|^2}{4} + \mu(x(s)) \right). \tag{1.12}$$

and the partition function $Q[\mu]$ becomes

$$Q[\mu] \propto A \int \mathcal{D}x(s) \exp\left(-E[x(s), 0, 1]\right) \delta(x(1)). \tag{1.13}$$

We now see why we used the scaling $W = \mu/\epsilon^2$: with this scaling the stretching energy and the potential energy μ in (1.12) are evidently of the same order. If, instead, the stretching energy would dominate, we would just get a random walk concentrated around the grafting surface. If the potential energy would dominate, the chains would be concentrated around the minimums of the potential. So we need the entropic stretching energy and the potential energy μ to be in competition to satisfy $\phi = 1$.

1.3.1 Strong stretching theory

Now if the brush is strongly stretched, i.e. if $\epsilon \ll 1$, the dominant contribution to the partition function $Q[\mu]$ comes from the paths that minimise their total energy. This is because the contributions from the paths with higher energy are exponentially suppressed as $\exp(-1/\epsilon^2)$ in (1.13), due to the factor $1/\epsilon^2$ in the energy.

The strong stretching theory (SST) approximates $Q[\mu]$ as an integral over these "ground state paths" only. The ground-state paths $x(s)$ obey the Euler-Lagrange equations of the energy (1.12), implying

$$\frac{1}{2}x''(s) - \partial_x \mu(x(s)) = 0. \tag{1.14}$$

This looks like Newton's second law, and indeed Milner et al. [4] used an analogy with classical mechanics to show that the SST approximation of the self-consistent field $\mu(x)$ and the ground-state paths $x(s)$ become

$$\mu(x) = -\frac{\pi^2 x^2}{16}, \tag{1.15a}$$

$$x(s) = x_0 \cos(\pi s/2). \tag{1.15b}$$

The expressions (1.15) are the solutions of (1.14), with boundary conditions $x(0) = x_0$, $x(1) = 0$ specifying where the chain begins and ends, and the assumption $x'(0) = 0$, i.e. the tension of the free end is neglected.

Now the ground-state paths should still give rise to a uniform ϕ. In the SST this fixes the distribution $g(x_0)$ of the endpoints of the ground-state paths as

$$g(x_0) = \frac{x_0}{\sqrt{1 - x_0^2}},$$

which was proven by Netz and Schick [5].

Using this end-segment distribution, we can compute the free energy F of the brush. Weighing the paths in (1.13) with $g(x_0)$ and using (1.15) and (1.7a) gives

$$\frac{F}{n} = \frac{\pi^2}{48\epsilon^2} \tag{1.16}$$

This is the final result of the SST: the SST approximation of the free energy.

1.4 The diffusion equations

In this section we describe a manner of calculating $\phi[\mu]$ and $Q[\mu]$ using diffusion equations. This leaves an inverse problem: we can check whether a field is the self-consistent field μ, but we cannot calculate μ directly.

To calculate $\phi[W]$ and $Q[W]$, we introduce the partial partition functions

$$q(x,s) \propto \int \mathcal{D}x(s) \exp\left(-E[x(s),0,s]\right) \delta(x(s)-x), \tag{1.17a}$$

$$q^\dagger(x,s) \propto \int \mathcal{D}x(s) \exp\left(-E[x(s),s,1]\right) \delta(x(s)-x)\, \delta(x(1)). \tag{1.17b}$$

where the energy E is given by (1.12). The locality of the energy (1.12) implies that these partial partition functions satisfy diffusion equations (see [10] for details). The substitution

$$q^*(x,s) = q^\dagger(x,1-s)$$

slightly simplifies these diffusion equations, giving

$$\partial_s q(x,s) = \left(\epsilon^2 \partial_x^2 - \frac{\mu(x)}{\epsilon^2}\right) q(x,s), \tag{1.18a}$$

$$\partial_s q^*(x,s) = \left(\epsilon^2 \partial_x^2 - \frac{\mu(x)}{\epsilon^2}\right) q^*(x,s). \tag{1.18b}$$

If the diffusion equations (1.18) are accompanied by suitable boundary conditions, we can calculate the partial partition functions q and q^* from the external field.

Combining the definitions (1.17) of the partial partition functions with the expressions (1.11b) for ϕ, (1.13) for Q and (1.7a) for F, we can calculate Q, ϕ and F from q and q^*:

$$Q = \int dx\, q(x,s)q^*(x,1-s), \tag{1.19a}$$

$$\phi(x) = \frac{1}{Q}\int_0^1 ds\; q(x,s)q^*(x,1-s). \tag{1.19b}$$

$$F = -\ln(Q) - \frac{1}{\epsilon^2}\int_0^1 dx\,\mu(x) \tag{1.19c}$$

The problem of the dry polymer brush reduces completely to the following: find the self-consistent field $\mu(x)$ such that the concentration (1.19b) is uniform, where $q(x,s)$ and $q^*(x,s)$ are determined by the diffusion equations (1.18) and their boundary conditions.

1.4.1 Boundary conditions

We only need to specify the relevant boundary conditions. Firstly, we have the initial conditions

$$q(x,0) = 1, \tag{1.20a}$$

$$q^*(x,0) = \sqrt{6}\epsilon\,\delta(x). \tag{1.20b}$$

The initial condition (1.20b) makes sure that one end of the polymer chain is constrained to $x = 0$. The initial condition (1.20a) does not constrain the other end of the polymer.

Secondly, we want to deal with the boundaries $x = 0$ and $x = 1$. The boundary

conditions at $x = 0$ and $x = 1$ are

$$\partial_x q(0, s) = \partial_x q^*(0, s) = 0,$$

$$\partial_x q(1, s) = \partial_x q^*(1, s) = 0.$$

These boundary conditions make sure that a polymer chain does not go through the boundaries $x = 0$ or $x = 1$. Therefore, together with the diffusion equations (1.18) they imply that Q (1.19a) is independent of s.

Chapter 2
Investigation of the diffusion equations with parabolic potential in the strong stretching limit

As we have seen in Section 1.3, in the case of the strongly stretched brush we can approximate the self-consistent field with a parabola. Recall that the self-consistent field μ was defined as the field that causes the segment density ϕ to be uniform. To see if the parabolic potential indeed approximately satisfies this self-consistency relation, we insert the parabolic potential (1.15a) into the diffusion equations (1.18). This gives the diffusion equations for the parabolic potential

$$\partial_s q(x,s) = \left(\epsilon^2 \partial_x^2 + \frac{\pi^2}{16\epsilon^2} x^2\right) q(x,s), \tag{2.1a}$$

$$\partial_s q^*(x,s) = \left(\epsilon^2 \partial_x^2 + \frac{\pi^2}{16\epsilon^2} x^2\right) q^*(x,s). \tag{2.1b}$$

In this chapter, we analyse (2.1) in the strong stretching limit $\epsilon \ll 1$ using both perturbative and numerical methods. Then we calculate the segment density ϕ from our asymptotic and numerical solution of q and q^*, to check if $\phi = 1$ is approximately satisfied.

2.1 Asymptotic solution

We start with the asymptotic solution. In Section 2.1.1 we transform the diffusion equations (2.1) in a manner very similar to the WKB approximation. Then in Section 2.1.2 and 2.1.3 we compute the asymptotic solution for the transformed variables, and in Section 2.1.4 we compute the asymptotic solution for the segment density ϕ.

2.1.1 Transforming the diffusion equations

We start with the transformation

$$q \equiv \exp(\sigma/\epsilon^2), \quad q^* \equiv \exp(\sigma^*/\epsilon^2), \tag{2.2}$$

giving the transformed diffusion equations

$$\partial_s \sigma = \epsilon^2 \partial_x^2 \sigma + (\partial_x \sigma)^2 + \frac{\pi^2}{16} x^2, \tag{2.3a}$$

$$\partial_s \sigma^* = \epsilon^2 \partial_x^2 \sigma^* + (\partial_x \sigma^*)^2 + \frac{\pi^2}{16} x^2, \tag{2.3b}$$

and the transformed boundary conditions

$$\sigma(x, 0) = 0, \tag{2.4a}$$

$$\lim_{s \to 0} \exp(\sigma^*(x, s)/\epsilon^2) = \sqrt{6}\epsilon\, \delta(x), \tag{2.4b}$$

$$\partial_x \sigma(0, s) = \partial_x \sigma^*(0, s) = 0, \tag{2.4c}$$

$$\partial_x \sigma(1, s) = \partial_x \sigma^*(1, s) = 0. \tag{2.4d}$$

To simplify our system further, we use the transform

$$u \equiv \partial_x \sigma, \quad u^* \equiv \partial_x \sigma^*. \tag{2.5}$$

Differentiating (2.3) with respect to x and using (2.4) gives

$$\partial_s u = \epsilon^2 \partial_x^2 u + 2u \partial_x u + \frac{\pi^2}{8} x \tag{2.6a}$$

$$u(0, s) = u(1, s) = u(x, 0) = 0 \tag{2.6b}$$

and a similar system for the starred variables

$$\partial_s u^* = \epsilon^2 \partial_x^2 u^* + 2u^* \partial_x u^* + \frac{\pi^2}{8} x, \tag{2.7a}$$

$$u^*(0, s) = u^*(1, s) = 0, \tag{2.7b}$$

and (2.4b) must also hold. After our two transformations (2.2) and (2.5) we can truly exploit the strong stretching $\epsilon \ll 1$: setting $\epsilon = 0$ in (2.6) and (2.7) gives two first-order scalar systems solvable using the method of characteristics.

Once we know u and u^*, we must recover σ and σ^* through

$$\sigma(x, s) = \int_{x_0}^{x} dr\, u(r, s) + c(x_0, s), \tag{2.8a}$$

$$\sigma^*(x, s) = \int_{x_0}^{x} dr\, u^*(r, s) + c^*(x_0, s), \tag{2.8b}$$

where $c(x_0, s)$, $c^*(x_0, s)$ are integration constants depending on s and the lower limit x_0 only. Using (2.3), (2.6) and (2.7), we can determine $c(x_0, s)$ and $c^*(x_0, s)$, giving

$$\sigma(x, s) = \int_{0}^{x} dr\, u(r, s) + \epsilon^2 \int_{0}^{s} dw\, \partial_x u(0, w), \tag{2.9a}$$

$$\sigma^*(x, s) = \int_{0}^{x} dr\, u^*(r, s) + \epsilon^2 \int_{0}^{s} dw\, \partial_x u(0, w) + c^*, \tag{2.9b}$$

where c^* is a constant determined by the condition (2.4b), and we have chosen $x_0 = 0$ for convenience. Next we can recover q and q^* using (2.2).

2.1.2 Asymptotic solution for u

We begin with the outer asymptotic solution for u. Expanding $u = u_0 + \epsilon^2 u_1 + \ldots$, we obtain

$$\partial_s u_0 - 2u_0 \partial_x u_0 = \frac{\pi^2}{8} x \tag{2.10}$$

with the same boundary conditions (2.6b). This is a first-order scalar PDE for u_0, which can therefore be solved exactly using the method of characteristics, giving

$$u_0(x,s) = \begin{cases} \frac{\pi}{4}\tan(\pi s/2)x & \text{for } x < \cos(\pi s/2), \\ \frac{\pi}{4}\sqrt{1-x^2} & \text{for } x > \cos(\pi s/2). \end{cases} \tag{2.11}$$

It is straightforward to check that these expressions indeed satisfy (2.10) and the boundary conditions (2.6b). In fact, for $x < \cos(\pi s/2)$ we have an exact solution of the full PDE (2.6a). This means we expect an exponentially small error for $x < \cos(\pi s/2)$. For $x > \cos(\pi s/2)$, we expect an error of order $\mathcal{O}(\epsilon^2)$.

Inner layer for u at $x = 1$

At $x = 1$ we find an inner layer for $u(x,s)$ of width $\epsilon^{4/3}$ and height $\epsilon^{2/3}$. Defining $x = 1 - \epsilon^{4/3}\xi$ and $u(x,s) = \epsilon^{2/3}v(\xi,s)$, we have the governing equation

$$\partial_\xi^2 v - 2v\partial_\xi v + \frac{\pi^2}{8} = 0, \tag{2.12a}$$

$$v(0,s) = 0, \qquad v(\xi,s) \sim \frac{\pi}{2\sqrt{2}}\sqrt{\xi} \text{ as } \xi \to \infty. \tag{2.12b}$$

We can now see why we had to choose a width $\epsilon^{4/3}$ and height $\epsilon^{2/3}$: this is the only way in which (2.6) gives a sensible dominant balance and $u(x,s) = \epsilon^{2/3}v(\xi,s)$ with v given by (2.12b) is $\mathcal{O}(1)$ as $\xi \to \infty$. This same line of reasoning will be used to determine the width and height of all other boundary layers.

A solution for v in terms of the Airy function can be found. The solution is

$$v(\xi,s) = -C_1\frac{\mathrm{Ai}'(C_1\xi - C_2)}{\mathrm{Ai}(C_1\xi - C_2)}$$

where $C_1 = \frac{1}{2}\pi^{2/3}$ and $C_2 = 4\pi^{-4/3}\partial_\xi v(0,s) \approx 1.019$ is defined by $\mathrm{Ai}'(-C_2) = 0$. Note that the differential equation is extremely sensitive to its initial conditions. Any larger

value $\partial_\xi v(0,s)$ will cause v to blow up for finite ξ, and any smaller value $\partial_\xi v(0,s) < C$ will cause v to behave as $-\sqrt{\xi}$ instead of $\sqrt{\xi}$. The inner solution at $x = 1$ becomes

$$u_{\text{inner}}(x,s) = -\epsilon^{2/3} C_1 \frac{\text{Ai}'\left(C_1\epsilon^{-4/3}(1-x) - C_2\right)}{\text{Ai}\left(C_1\epsilon^{-4/3}(1-x) - C_2\right)} \tag{2.13}$$

valid when $1 - x = \mathcal{O}(\epsilon^{4/3})$.

We can combine the inner solution (2.13) with the outer solution (2.11) into a partial composite solution. We say partial, because we can only expect this partial composite solution to be valid away from the other inner layers that we will discuss shortly. The partial composite solution is the sum of the outer (2.11) and inner (2.13) solutions minus their common limit (2.12b) i.e.

$$u_{\text{comp}}(x,s) = u_{\text{inner}}(x,s) + \frac{\pi}{4}\sqrt{1-x^2} - \frac{\pi}{2\sqrt{2}}\sqrt{1-x}. \tag{2.14}$$

This is valid when $x > \cos(\pi s/2)$ and s is not close to either 0 or 1.

Inner layer for u at $x = \cos(\pi s/2)$

At $x = \cos(\pi s/2)$ we find a corner layer for $u(x,s)$ of width ϵ and height ϵ. Defining $x = \cos(\pi s/2) + \epsilon\xi$ and $u(x,s) = \frac{\pi}{4}(\sin(\pi s/2) + \epsilon v(\xi,s))$, we have the governing equation

$$\partial_s v = \partial_\xi^2 v + \frac{\pi}{2} v \partial_\xi v + \frac{\pi}{2}\xi, \tag{2.15a}$$

$$v(\xi,s) \sim \tan(\pi s/2)\xi \text{ as } \xi \to -\infty,\ v(\xi,s) \sim -\cot(\pi s/2)\xi \text{ as } \xi \to \infty. \tag{2.15b}$$

Unfortunately, we have not found an analytic solution for this inner layer.

Breakdown of the corner layer for u

We expect our analysis (2.15) of the corner layer to break down when x approaches the boundaries $x = 0$ and $x = 1$. The reason is that at least (2.15b) cannot hold

anymore: near $x = 0$ we have the boundary condition for $u(x = 0, s) = 0$ instead, and near $x = 1$ we have the boundary layer (2.12).

Near $x = 0$ it will break down around $(x, s) = (0, 1)$ where $x = \cos(\pi s/2) = \mathcal{O}(\epsilon)$ since the corner layer has width ϵ. This translates into $x = \mathcal{O}(\epsilon)$ and $1 - s = \mathcal{O}(\epsilon)$. So the area where the corner layer breaks down near $x = 0$ is $\mathcal{O}(\epsilon^2)$.

Near $x = 1$ it will break down around $(x, s) = (1, 0)$ where $1-x = 1-\cos(\pi s/2) = \mathcal{O}(\epsilon)$ since the corner layer has width ϵ and the inner layer at $x = 1$ has relatively negligible width $\epsilon^{4/3}$. This translates into $1 - x = \mathcal{O}(\epsilon)$ and $s = \mathcal{O}(\epsilon^{1/2})$. So the area where the corner layer breaks down near $x = 1$ is $\mathcal{O}(\epsilon^{3/2})$.

2.1.3 Asymptotic solution for u^*

Next we deal with the outer asymptotic solution for u^*. Expanding $u^* = u_0^* + \epsilon^2 u_1^* + \ldots$ gives

$$\partial_s u_0^* - 2u_0^* \partial_x u_0^* = \frac{\pi^2}{8} x, \tag{2.16a}$$

$$u_0^*(0, s) = u_0^*(1, s) = 0, \tag{2.16b}$$

So u_0^* is governed by exactly the same PDE as u_0, but with different boundary conditions. We start the characteristics from $u_0^*(x = s = 0) = v$ with v a real variable, this yields the solution

$$u_0^*(x, s) = -\frac{\pi}{4} x \cot(\pi s/2). \tag{2.17}$$

In fact this exactly solves (2.7a), but it does not agree with the boundary condition $u_0^*(1, s) = 0$, suggesting a boundary layer at $x = 1$. Away from this boundary layer we expect an exponentially small error.

Inner layer for u^* at $x = 1$

Indeed we find a boundary layer at $x = 1$ of width ϵ^2 and height 1 with governing equation

$$\partial_\xi^2 u_0^* + 2u_0^* \partial_\xi u_0^* = 0, \tag{2.18a}$$

$$u_0^*(\xi, s) \sim -\frac{\pi}{4} \cot(\pi s/2) \text{ as } \xi \to -\infty \tag{2.18b}$$

where $x = 1 + \epsilon^2 \xi$. Therefore we get inner solutions of the type

$$u_{\text{inner}}^* = -f(s) \tanh(f(s)(1 - x)/\epsilon^2).$$

We can match this with the outer solution using Van Dyke's rule, giving

$$u_{\text{inner}}^* = -\frac{\pi}{4} \cot(\pi s/2) \tanh\left(\frac{\pi}{4} \cot(\pi s/2)(1 - x)/\epsilon^2\right) \tag{2.19}$$

valid when $1 - x = \mathcal{O}(\epsilon^2)$.

Again we combine the inner solution (2.19) with the outer solution (2.17) into a composite solution. The composite solution is the sum of the outer (2.17) and inner (2.19) solutions minus their common limit (2.18b) i.e.

$$u_{\text{comp}}^*(x, s) = u_{\text{inner}}^*(x, s) - \frac{\pi}{4}(x - 1) \cot(\pi s/2). \tag{2.20}$$

2.1.4 Asymptotic solution for ϕ

In this section we approximate ϕ using the outer asymptotic solutions for u and u^*. To do this, we first have to approximate σ and σ^*, and then q and q^*.

We approximate σ and σ^* by inserting the outer asymptotic solutions for u and

u^* into (2.9a) and (2.9b). This gives

$$\sigma_0(x,s) = \begin{cases} \frac{\pi}{8}\tan(\pi s/2)x^2 - \frac{\epsilon^2}{2}\log\left(\cos(\pi s/2)\right) & \text{for } x < \cos(\pi s/2), \\ \frac{\pi}{8}\left(x\sqrt{1-x^2} + \arcsin(x) + \frac{\pi}{2}(s-1)\right) & \text{for } x > \cos(\pi s/2), \end{cases} \tag{2.21}$$

and

$$\sigma_0^*(x,s) = -\frac{\pi}{8}\cot(\pi s/2)x^2 - \frac{\epsilon^2}{2}\log(4\sin(\pi s/2)/3) \tag{2.22}$$

For σ^*, we have taken care to agree with the delta function boundary condition (2.4b). To estimate the error of this approximation, we note that σ and σ^* are integrals over u and u^* so we need to use our understanding of the errors in the asymptotic solutions for u and u^*.

Firstly for u when $x < \cos(\pi s/2)$ we have an exact solution of the outer problem so we expect an exponentially small error away from the corner layer. For x larger than $\cos(\pi s/2) - \mathcal{O}(\epsilon)$ we have to integrate over the corner layer giving an order $\mathcal{O}(\epsilon^2)$ error. So we have

$$|\sigma - \sigma_0|(x,s) = \begin{cases} E.S.T. & \text{for } x < \cos(\pi s/2) - \mathcal{O}(\epsilon), \\ \mathcal{O}(\epsilon^2) & \text{for } x > \cos(\pi s/2) - \mathcal{O}(\epsilon), \end{cases} \tag{2.23}$$

For σ^* we reason in the same way. Away from the inner layer at $x = 1$ we expect an exponentially small error, but for x close to 1 we have to integrate over the inner layer at $x = 1$ giving an order $\mathcal{O}(\epsilon^2)$ error. So we have

$$|\sigma^* - \sigma_0^*|(x,s) = \begin{cases} E.S.T. & \text{for } x < 1 - \mathcal{O}(\epsilon^2), \\ \mathcal{O}(\epsilon^2) & \text{for } x > 1 - \mathcal{O}(\epsilon^2), \end{cases} \tag{2.24}$$

Next we approximate q by inserting (2.21) and (2.22) into (2.2) which gives

$$q_0(x,s) = \begin{cases} (1/\sqrt{\cos \pi s/2}) \exp\left(\frac{\pi}{8\epsilon^2} \tan(\pi s/2) x^2\right) & \text{for } x < \cos(\pi s/2), \\ (1/\sqrt{\cos \pi s/2}) \exp\left[\frac{\pi}{8\epsilon^2}\left(x\sqrt{1-x^2} + \arcsin(x) + \frac{\pi}{2}(s-1)\right)\right] & \text{for } x > \cos(\pi s/2). \end{cases} \tag{2.25}$$

and

$$q_0^* = \sqrt{3/(4\sin(\pi s/2))} \exp\left(-\frac{\pi}{8\epsilon^2} \cot(\pi s/2) x^2\right) \tag{2.26}$$

Note the similarity between q_0^* and q_0 for $x < \cos(\pi s/2)$. They are the same except for a phase shift due to the different boundary conditions.

Using these asymptotic solutions q_0 and q_0^* we can finally compute the asymptotic solutions for Q and ϕ. Firstly, we compute Q by inserting (2.25) and (2.26) in (1.19a). Since the diffusion equations imply that Q does not depend on s, we can substitute $s = 0$ and compute

$$Q_0 = \int_0^1 dx\, q_0^*(x,1) = \sqrt{3}/2. \tag{2.27}$$

Next we compute the asymptotic solution for ϕ by inserting (2.25) and (2.26) in (1.19b). The resulting integral cannot be solved analytically, so we used Laplace's method to find the asymptotic approximation

$$\phi_0(x) = \frac{2}{\pi} \log\left(\frac{1+\sqrt{1-x^2}}{x}\right). \tag{2.28}$$

Here a term $\mathcal{O}(\epsilon)$ has already been ignored, but we there is another error due to the errors (2.23) and (2.24). The order $\mathcal{O}(\epsilon^2)$ errors in σ and σ^* might be worrying: inserting them in $q = \exp(\sigma/\epsilon^2)$ and $q^* = \exp(\sigma^*/\epsilon^2)$ gives order $\mathcal{O}(1)$ multiplicative errors in q and q^*. Nevertheless, it turns out that because the $\mathcal{O}(\epsilon^2)$ errors are restricted to the region $x > \cos(\pi s/2) - \mathcal{O}(\epsilon)$, our asymptotic solutions Q_0 and ϕ_0

are still correct. To be specific we get

$$Q = \sqrt{3}/2 + \mathcal{O}(\epsilon^2), \tag{2.29a}$$

$$\phi(x) = \frac{2}{\pi} \log\left(\frac{1+\sqrt{1-x^2}}{x}\right) + \mathcal{O}(\epsilon). \tag{2.29b}$$

These error estimates should be taken with a grain of salt. In deriving them we have ignored the breakdown of the corner layer described on Page 21. The expected impact of this is that the error in Q is $\mathcal{O}(\epsilon)$ and that the error in $\phi(x)$ is larger near 0 and 1 where the corner layer breakdown matters.

Lastly, inserting our expression (2.29a) for Q into (1.19c) gives

$$\frac{F}{k_B T} = \frac{\pi^2}{48\epsilon^2} - \ln\left(\frac{\sqrt{3}}{2}\right) + \mathcal{O}(\epsilon^2).$$

Most importantly, the dominant term proportional to $1/\epsilon^2$ agrees with the SST approximation (1.16). Note however, that this agreement is not unexpected: the dominant term agrees just because we have used the parabolic potential.

2.2 Numerical solution

To check our asymptotic solutions, we solve the diffusion equations (2.3) for σ and σ^* numerically. To do this, we must first approximate the delta function in the initial condition (2.4b), which we do with a narrow Gaussian of width a, i.e.

$$\delta(x) \to \frac{1}{\sqrt{\pi}a} \exp\left(-\frac{x^2}{a^2}\right). \tag{2.30}$$

This implies the following initial condition for $\sigma^*(x,0)$:

$$\sigma^*(x,0) = -\epsilon^2 \frac{x^2}{a^2} + \epsilon^2 \ln\left(\frac{\sqrt{6}\epsilon}{\sqrt{\pi}a}\right). \tag{2.31}$$

We then use the backward time, centred space method to solve (2.3) with the modified initial condition (2.31). So, rewriting the diffusion equations as $\partial_s \sigma(x,s) = F(\sigma(x,s))$, we use the backward Euler method

$$\sigma(x,s) = \sigma(x, s-\Delta s) + \Delta s\, \hat{F}(\sigma(x,s)) \tag{2.32}$$

to find $\sigma(x,s)$ from $\sigma(x, s-\Delta s)$. Here $\hat{F}$ approximates F by replacing the x-derivatives with finite central differences. For each time step Δs, the non-linear equation (2.32) is solved using Newton's method. We terminate Newton's method once the residual of (2.32) is smaller than 10^{-9} for each x.

Once σ and σ^* have been computed, we compute the other relevant variables u, u^*, Q and ϕ with the formulas in Sections 1.4 and 2.1.1. Integration is implemented with the trapezoidal rule.

The numerical values we have used are

$$\epsilon = 0.05, 0.1, 0.2, \quad a = \epsilon/20, \quad \Delta x = a/5, \quad \Delta s = 10^{-4} \tag{2.33}$$

except for σ^* we use $\Delta s = 10^{-6}$ when $s < 0.02$.

2.3 Comparison of asymptotic and numerical solutions

Now we compare our asymptotic solutions of Section 2.1 with the numerical solutions of Section 2.2.

To accurately compare our asymptotic solutions with our numerical solutions, we

should incorporate the delta function approximation (2.30). This does not affect u, σ or q, but we should solve for u^*, σ^* and q^* again with the adapted initial condition (2.31). Luckily, the asymptotic solution changes only slightly: for each s in u^* (2.17), u^*_{comp} (2.20), σ^* (2.22) and q^* (2.26) we just have to do the replacement

$$s \to s + (a/2\epsilon)^2. \tag{2.34}$$

In principle, this correction to our asymptotic solution for q^* also affects the asymptotic solution for Q and ϕ. These corrections are harder to compute, so we stick with (2.27) and (2.28). In light of the approximation (2.30) and the correction (2.34) we should actually, computationally, consider the limit $a/\epsilon \to 0$. However, we will see that the choice $a/\epsilon = 1/20$ already gives excellent agreement with the asymptotic solutions for ϕ.

Furthermore, whenever we present relative differences, we plot the difference divided by the average. So the relative difference between f_1 and f_2 is plotted as $(f_1 - f_2)/\frac{1}{2}(f_1 + f_2)$.

2.3.1 Comparison of the segment density

We start with the most important quantity: the segment density ϕ. Figure 2.1a shows a plot of the asymptotic solution (2.28) and the numerical calculations. Figure 2.1b shows the relative difference between the two. The relative difference becomes large ($\geq 5\%$) only for x close to either 0 or 1 and clearly decreases as $\epsilon \to 0$.

2.3.2 Comparison of the outer solutions for u and u^*

Next we compare the numerical and outer asymptotic solutions for $u(x, s)$ and $u^*(x, s)$ in Figure 2.2. We plotted the outer asymptotic solutions given by (2.11) for u and

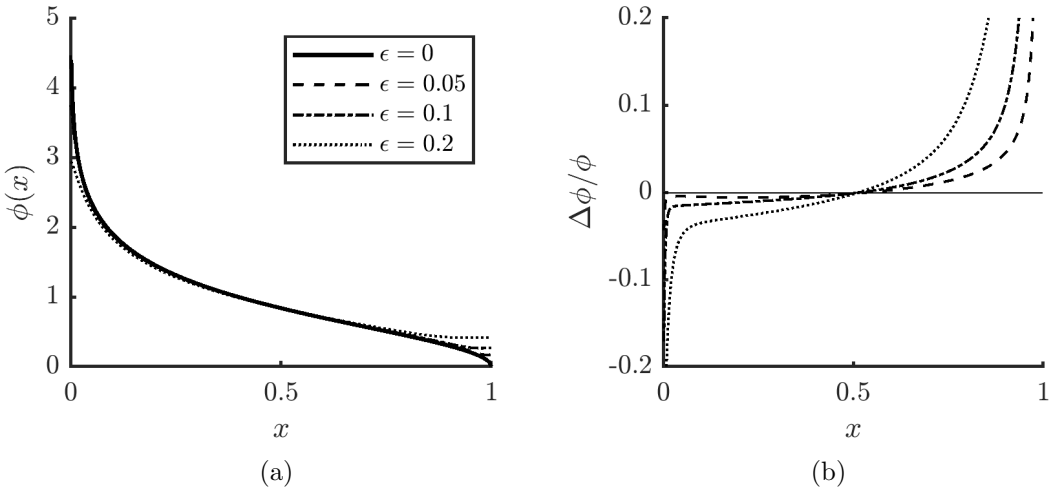

Figure 2.1: (a) A plot of the perturbative ($\epsilon = 0$) and numerical approximations of the segment density $\phi(x)$. The segment density $\phi(x)$ becomes large as $x \to 0$ and vanishes as $x \to 1$. (b) Relative difference between the numerical and perturbative approximations of the segment density $\phi(x)$. The thin horizontal line is just a reference zero line.

(2.17) for u^*, and have incorporated the correction (2.34) for u^*. We have chosen to plot u and u^* at fixed $x = 0.5$ or fixed $s = 0.5$, where our asymptotic approximations should be relatively accurate, because this is away from the boundary layers at $s = 0$, $s = 1$ and $x = 1$. In all figures, the agreement clearly becomes better as ϵ decreases.

Firstly, in Figure 2.2a we see $u(x, s)$ at fixed $x = 0.5$ as a function of s. The agreement is particularly good for $s < 0.5$, while around $s \approx 0.65$ we see the corner layer (2.15). In Figure 2.2c we have plotted $u(x, s)$ at fixed $s = 0.5$ as a function of x. Again for small $x < 0.5$ the agreement is particularly good, and we see the corner layer around $x \approx 0.7$. Around $x = 1$ we might see the boundary layer (2.12), although on this scale the agreement is quite good.

Secondly, in Figure 2.2b we see $u^*(x, s)$ at fixed $x = 0.5$ as a function of s. The results are practically indistinguishable. In Figure 2.2d we have plotted $u^*(x, s)$ at fixed $s = 0.5$ as a function of x. Away from $x = 1$ the results are indistinguishable, while near $x = 1$ we clearly see the boundary layer (2.18).

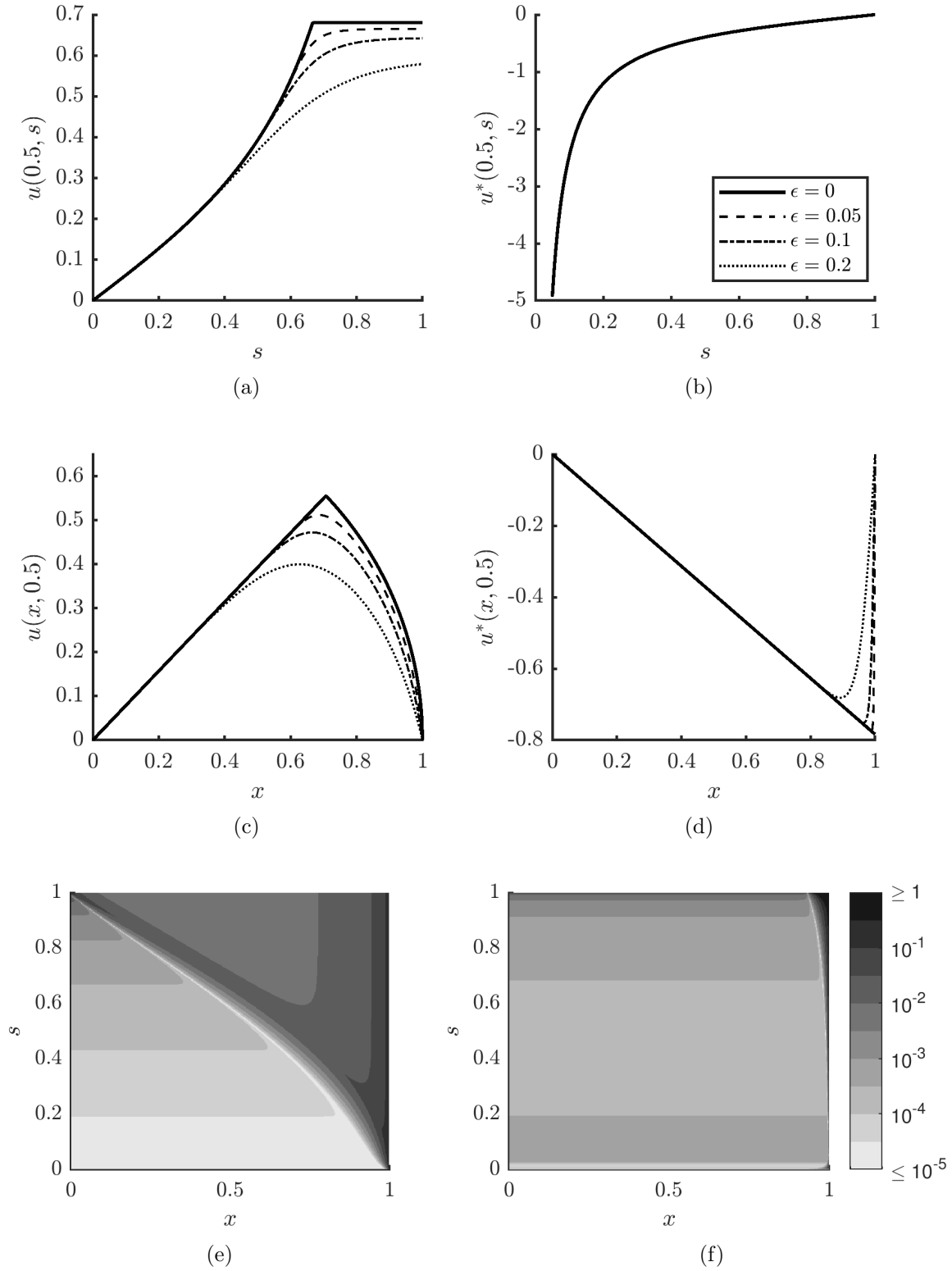

Figure 2.2: (a-d) $u(x, s)$ and $u^*(x, s)$ at fixed $x = 0.5$ or fixed $s = 0.5$. (e-f) Absolute relative difference between the outer approximation of $u(x, s)$ (e) or $u^*(x, s)$ (f) and the numerical results for $\epsilon = 0.05$. The relative difference is shown as a greyscale where lighter is smaller (see colourbar).

Finally in Figure 2.2e and 2.2f we have plotted the absolute relative difference between the outer perturbative expansions and numerical results for $\epsilon = 0.05$. In Figure 2.2e we clearly see the corner layer at $x = \cos(\pi s/2)$ and the boundary layer at $x = 1$. Within the corner layer, the difference is largest for $(x, s) = (0, 1)$ and $(x, s) = (1, 0)$, which is in line with the discussion on Page 21. In Figure 2.2f we also clearly see the boundary layer at $x = 1$. Furthermore, it is reassuring that, except for these thin inner layers, the numerical and perturbative approximations agree quite well.

2.3.3 Comparison of composite solutions

In Figures 2.3a and 2.3b we have plotted the results for the composite approximation (2.14) of u and (2.20) of u^* for fixed $s = 0.5$ and near $x = 1$. Again we have incorporated the correction (2.34) for u^*. The composite solution is in both cases a clear improvement over the outer solution. For u, the partial composite solution (2.14) becomes worse for smaller x, but this is to be expected. As x decreases it gets closer to the corner layer (2.15), which is not included in this partial composite solution.

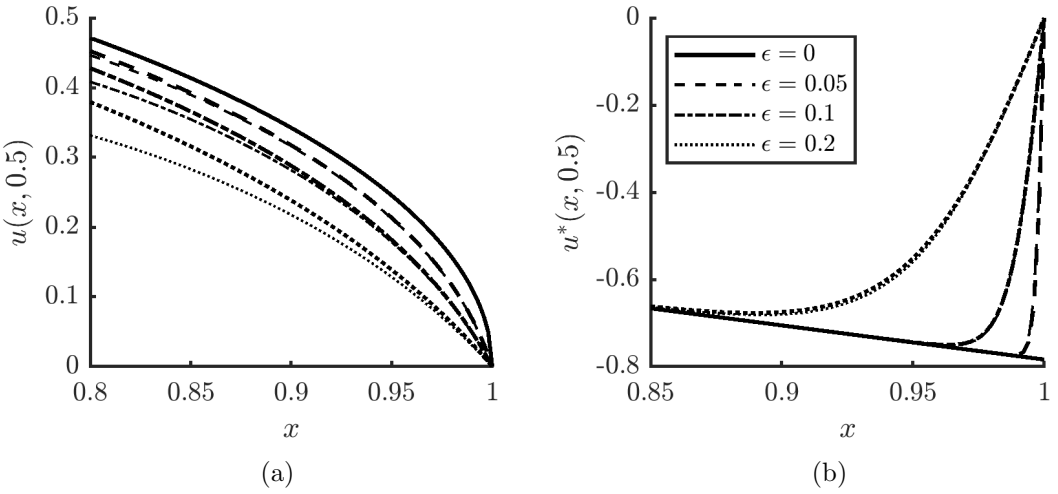

Figure 2.3: Composite approximation of $u(x, s)$ and $u^*(x, s)$ at fixed $s = 0.5$. The bold lines are the perturbative results, the light lines are the numerical results. The bold line labelled $\epsilon = 0$ is the outer approximation.

Chapter 3
Discussion and outlook

In the previous chapter we have calculated the segment density $\phi(x)$ that results from the SST parabolic potential, to test whether indeed $\phi \approx 1$. Perturbative and numerical methods agreed on the result shown in Figure 2.1a: the segment density becomes large as $x \to 0$ and vanishes as $x \to 1$. To emphasise: the parabolic potential does not almost satisfy the self-consistency relation $\phi = 1$, in fact the segment density is far from uniform. So what went wrong? Why does the parabolic potential not work?

3.1 Re-examining the parabolic potential

Firstly, we might go back to the original justification of the parabolic potential in the SST of Section 1.3. We could object that the parabolic potential is only valid within the SST (i.e. where only the ground-state paths are considered) and that it therefore is not sensible to transfer the parabolic potential directly into the diffusion equations of SCFT (where fluctuations around ground-state paths are considered). Indeed, it is not clear a priori why the SST self-consistent field and the SCFT self-consistent field should have any relation.

Nevertheless, Matsen showed [8], numerically, that the SCFT self-consistent field converges to the parabolic potential in the strong stretching limit $\epsilon \to 0$, although the convergence is not uniform. More precisely, he showed that the deviation from the parabolic potential is well-described by three corrections. The first two are referred to as the "proximal layer" and were discovered by Likhtman and Semenov [6]. The last was discovered by Matsen [7] and Matsen calls it either the "full classical theory" or the "entropy due to free ends". Each correction can be thought of as being of order $\mathcal{O}(\epsilon^2)$ either in width or in height.

Likhtman and Semenov's first correction is simply $\epsilon^2\delta(x)$ so a delta function [6]. The second correction has no analytic formula yet, but numerically has height $ord(1)$ and vanishes for $x \gg \epsilon^2$ [6] so it has width $\mathcal{O}(\epsilon^2)$.

Matsen's "full classical theory" correction is seen to be a global correction vanishing as $\epsilon \to 0$ [7]. Although he does not specify the order of this correction, he does show that the parameter v_0^2 that controls it has order $\mathcal{O}(\epsilon^2)$ [7], which makes it plausible that this last full classical theory correction has order $\mathcal{O}(\epsilon^2)$ as well.

This seems to be a contradiction: Matsen showed numerically that the SCFT self-consistent field converges to the parabolic potential, while we showed that the parabolic potential gives rise to a far from uniform segment density. Assuming Matsen's numerical evidence is correct, the only possible conclusion is that corrections to the parabolic potential still have an important effect on the segment density ϕ.

With our asymptotic analysis we can in fact explain why corrections of the parabolic potential of order $\mathcal{O}(\epsilon^2)$ impact the segment density. The segment density is directly determined by the partial partition functions q and q^*, which in our analysis are expressed as $q = \exp(\sigma/\epsilon^2)$ and $q^* = \exp(\sigma^*/\epsilon^2)$. The quantities σ and σ^* are in turn determined by the potential through diffusion equations. Therefore, order $\mathcal{O}(\epsilon^2)$ corrections of the parabolic potential will cause order $\mathcal{O}(\epsilon^2)$ corrections to both σ and σ^*. These, in turn, will cause order $\mathcal{O}(1)$ multiplicative corrections to q and q^*. Since q and q^* directly determine the segment density ϕ, it is clear that order $\mathcal{O}(\epsilon^2)$ corrections to the parabolic potential will have an important effect on the segment density.

3.2 Outlook

Ideally, we would like to use perturbation theory to predict the finite stretching corrections and the parabolic potential itself. An ideal perturbative scheme would go somewhat like this: expand the self-consistent field $\mu(x) = \mu_0(x) + \mu_1(x)\epsilon^2 + \ldots$, then solve the diffusion equations up to some desired order, then check up to what order the self-consistency condition $\phi(x) = 1$ can be satisfied. This should constrain $\mu_0(x), \mu_1(x), \ldots$, ideally giving the parabolic potential and, incrementally, smaller finite stretching corrections.

Such a scheme could provide an analytic and systematic manner of generating or estimating finite stretching corrections. These corrections could then also be used as asymptotic evidence that SCFT converges to SST in the strong stretching limit. It is clear that such a perturbative scheme could be very fruitful.

In this thesis, we have taken the first step in this perturbative scheme. We have assumed that $\mu_0(x)$ is parabolic (supported by numerical evidence [8]), and checked if $\phi(x) = 1$ was satisfied at least approximately. The answer, surprisingly, was that ϕ was very far from uniform. We concluded that finite stretching corrections have a large influence on ϕ.

To continue, we need to include finite stretching corrections of order up to $\mathcal{O}(\epsilon^2)$, and find all order $\mathcal{O}(\epsilon^2)$ corrections to σ and σ^*, before we can approximately satisfy $\phi = 1$. Our work on the outer solutions of u and u^*, as well as on their inner layers, will be valuable for this more general problem. Our outer asymptotic solution will likely remain the outer asymptotic solution of the more general problem, and our inner layer analysis at $x = 1$ will likely still apply, especially considering that Likhtman and Semenov's proximal layer is concentrated at $x = 0$.

References

[1] S. F. Edwards. "The statistical mechanics of polymers with excluded volume". In: *Proceedings of the Physical Society* 85.4 (1965), p. 613.

[2] K. M. Hong and J. Noolandi. "Theory of inhomogeneous multicomponent polymer systems". In: *Macromolecules* 14.3 (1981), pp. 727–736.

[3] A. Semenov. "Contribution to the theory of microphase layering in block-copolymer melts". In: *Zh. Eksp. Teor. Fiz* 88.4 (1985), pp. 1242–1256.

[4] S. T. Milner, T. A. Witten, and M. E. Cates. "Theory of the grafted polymer brush". In: *Macromolecules* 21.8 (1988), pp. 2610–2619.

[5] R. R. Netz and M. Schick. "Polymer brushes: from self-consistent field theory to classical theory". In: *Macromolecules* 31.15 (1998), pp. 5105–5122.

[6] A. E. Likhtman and A. N. Semenov. "An advance in the theory of strongly segregated polymers". In: *EPL (Europhysics Letters)* 51.3 (2000), p. 307.

[7] M. W. Matsen. "Corrections to the strong-stretching theory of polymer brushes due to the entropy of the free ends". In: *The Journal of chemical physics* 117.5 (2002), pp. 2351–2358.

[8] M. W. Matsen. "Investigating the dominant corrections to the strong-stretching theory for dry polymeric brushes". In: *The Journal of chemical physics* 121.4 (2004), pp. 1938–1948.

[9] G. Fredrickson. *The equilibrium theory of inhomogeneous polymers*. Online; accessed 4-December-2018. Oxford University Press, 2005. DOI: "10.1093/acprof:oso/9780198567295.001.0001".

[10] M. W. Matsen. "Self-consistent field theory and its applications". In: *Soft Matter*. Ed. by G. Gompper and M. Schick. Vol. 1: Polymer Melts and Mixtures. 2006.